Chalcogenide Letters Vol. 21, No. 7, July 2024, p. 557 - 565

Impact of different rinsing temperatures on SnS thin films created using the SILAR technique

Y. Qachaou[a,*], O. Daoudi[b], I. Jellal[a], A. Fahmi[a], M. Lharch[a], A. Qachaou[a], A. Raidou[a], M. Fahoume[a]
[a]*Laboratory of Materials Physics and Subatomic, Department of Physics, Faculty of Science, Ibn Tofail University, Kenitra Morocco*
[b]*Laboratory of Engineering and Materials (LIMAT), Faculty of Sciences Ben M'sik, Hassan II University of Casablanca, Morocco*

The (SnS) thin films were prepared by Successive Ionic Layer Adsorption and Reaction (SILAR), a versatile and simple method. The cationic and anionic solutions $SnCl_2.2H_2O$ and $Na_2S.9H_2O$ respectively were used as precursor materials, which will be deposited on glass substrates to study the effect of rinsing temperature on the properties of our thin films. The structural, morphological, and optical properties were investigated by using X-ray diffraction, Energy Dispersive X-ray analysis (EDX), Scanning Electron Microscopy (SEM) and spectrophotometer. X-ray Diffraction (XRD) patterns indicated that the deposited SnS thin films have an orthorhombic crystal structure. Uniform deposition of the material over the entire glass substrate was shown by Scanning Electron Microscopy (SEM). The optical band gap energy ranged from 1.5 to 1.82eV for direct transitions and from 0.6 to 0.95eV for indirect transitions.

(Received April 16, 2024; Accepted July 19, 2024)

Keywords: Tin sulphide, SILAR, Thin films, Rinsing temperature

1. Introduction

Due to an abundance of fossil resources currently, the current energy perspectives are not as optimistic regarding fossil fuels. The current energy outlook is less optimistic about fossil fuels, forcing our civilization to turn to new technological solutions such as renewable energies. Renewable energy is an energy using natural elements like Photovoltaic (PV), geothermal, and wind energy, they are free and respectful of the environment.

Photovoltaics (PV) have been recognized as a favorable option for generating clean and affordable energy for society. In light of this, considerable attention has been directed towards identifying cost-effective and environmentally safe materials.

Tin monosulfide has emerged as a strong contender, meeting various criteria, and establishing itself as a practical material for use in solar energy applications [1]. Its components, tin, and sulfur, are cost-effective, widely available, and environmentally friendly. While the binary compound SnS has a cubic structure [2], it also exhibits an orthorhombic structure [3]. This makes SnS well-suited for solar applications, with both indirect and direct optical band gaps. The indirect band gap ranges from 1 to 1.1 eV, and the direct band gap falls between 1.3 and 1.5 eV. Additionally, SnS thin films exhibit a significant absorption coefficient ($>10^5$ cm^{-1}) beyond the absorption edge, indicating their strong ability to absorb light even at higher wavelengths [4].

Thin films of SnS can be produced utilizing a range of physical and chemical techniques, including RF sputtering [5], thermal evaporation [6], Chemical bath deposition (CBD) [7], electrodeposition [8], spray pyrolysis [9], and the SILAR method [10], which is used in this work. The rinsing temperature has a significant impact on the structural and optical properties of thin films. It can influence the preferential orientation of grains in thin films. In our work, a rinsing temperature of 60°C promotes a stronger preferential orientation (higher TC_{hkl}), which can improve certain

* Corresponding author: qachaou.yussef@gmail.com
https://doi.org/10.15251/CL.2024.217.557

properties of the films. The rinsing temperature can also affect the size and distribution of grains in the thin films, which in turn can influence the optical and structural properties.

2. Experimental procedures

2.1. Synthesis of SnS

To prepare SnS thin films using the SILAR method, we started by using a cationic solution of $SnCl_2 + 2H_2O$ and an anionic solution of $Na_2S + 9H_2O$. The concentrations of tin chloride and sodium sulfide were fixed at 0.2M each and dissolved separately in 100 ml of distilled water. Before we begin the deposition process, we made sure to clean the substrates thoroughly. We used acetone for 10 minutes, followed by rinsing with distilled water and then washing them in an ethanol bath for another 10 minutes. After a final rinse with distilled water, we allowed the substrates to dry before proceeding with the SILAR method deposition.

During the deposition process, we immersed the substrates in the cationic solution ($SnCl_2$+$2H_2O$) for 20 seconds, which led to the adsorption of tin ions onto the surface. Next, we gently rinsed the substrates with distilled water for about 10 seconds to ensure the removal of any remaining solution. Afterward, we carefully dipped the substrates into the anionic solution (Na_2S+$9H_2O$) for about 20 seconds. This allowed the sulphide ions to interact with the tin ions that were earlier attached to the active spots on the substrate. Afterward, we gave the substrates another gentle rinse in distilled water for about 10 seconds. This step was important to ensure that any ions loosely clinging to the substrate were completely removed [11].

So, we completed the initial growth cycle using the SILAR method. We then went on to repeat this cycle a total of 40 times. This meticulous repetition was crucial to ensure that the thin films were deposited thoroughly and consistently each time.

During the SILAR method, several key parameters affect the thin film formation, including solution concentrations, temperature, immersion duration, and solution pH. In our study, we conducted experiments at varying rinsing temperatures: 60°C, 70°C, and 80°C, each corresponding to samples ech1, ech2, and ech3, respectively, while ensuring continuous stirring of the solution.

2.2. Mechanism of the reaction

The chemical reaction of SnS thin film growth by SILAR method is written as follows:

$$SnCl_2 + Na_2S \longrightarrow SnS + 2NaCl \quad (1)$$

2.3. Characterization

In our laboratory investigations, we employed various techniques like X-ray diffraction (XRD) to study the structure, scanning electron microscopy (EDX-SEM) to analyze the surface, and Raman spectroscopy to examine optical vibrational modes. Additionally, we measured the band gap energy using the Spectrophotometer (PerkinElmer Instrument Lambda 900 UV/Vis/NIR).

3. Results and discussion

3.1. Structural studies

Figure 1 shows us the X-ray diffraction (XRD) patterns of SnS thin films that have been carefully grown on glass substrates at different rinsing temperatures: 60°C, 70°C, and 80°C. We conducted a comparison between the observed interplanar distance values in these XRD spectrums and those obtained from a standard reference (JCPDS 00-001-0984). This analysis aimed to confirm the presence of the SnS phase characterized by an orthorhombic crystal structure, with no indication of secondary phases. The notable peaks observed in the XRD spectrum, which are associated with the SnS phase, included (012), (102), (110), (013), (104), (015), (006), (115), (212), (204), and (125). The lack of extra peaks confirms the purity of the crystalline structure, indicating the absence of secondary phases.

The relationship among the interplanar distance (d_{hkl}), the lattice plane index (hkl), and the lattice parameters for the orthorhombic crystal can be articulated as follows [12]:

$$\frac{1}{d_{hkl}^2} = \frac{h^2}{a^2} + \frac{k^2}{b^2} + \frac{l^2}{c^2} \quad (2)$$

We calculated the lattice parameters "a," "b," and "c" for the orthorhombic structure of the deposited films, resulting in values of a = 4.04 Å, b = 4.1 Å, and c = 11.4 Å. Our calculated values are very close to the reported values, indicating a strong agreement between our findings and existing data [13].

We used XRD data to calculate the size of the crystals, the density of dislocations (δ), and the level of microstrain (ε) in the samples. These calculations were performed using the following mathematical formulas [14]:

Crystallite size: $$D = \frac{0.9\,\beta}{\lambda\ cos\theta} \quad (3)$$

Dislocation density: $$\delta = \frac{1}{D^2} \quad (4)$$

Micro strain: $$\varepsilon = \frac{\beta\ cos\theta}{4} \quad (5)$$

In this equation, D symbolizes the size of the grains, λ represents the wavelength of the Cu-Kα radiation (λ=1.5405 Å), β signifies the experimentally measured width of the diffraction peak at half-maximum intensity (FWHM), and θ stands for the Bragg angle.

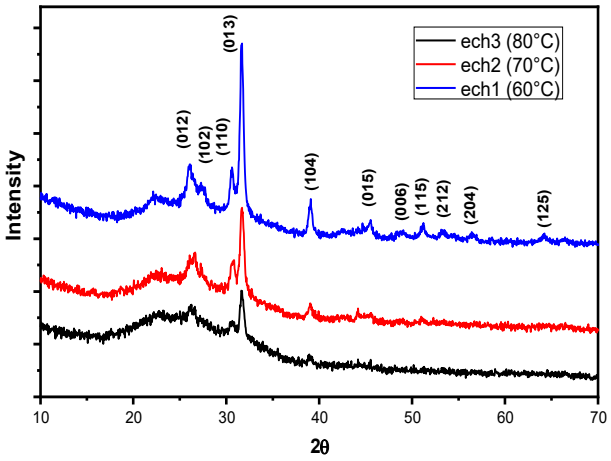

Fig. 1. XRD spectra of films at different of distilled water.

Think of it like this: when we look at the XRD pattern of thin films, we often notice that the intensity ratios of different peaks don't match exactly with what we expect from the JCPDS file, which is usually obtained from powder samples. This mismatch happens because the grains in the thin films grow in a textured way, aligning themselves along the substrate. This alignment is influenced by how the deposition process is carried out. To help us understand this better, we use something called the texture coefficient. It's like a special tool that tells us about the direction in which the deposited films are growing. We calculate this coefficient using the equation provided below [15].

$$TC_{hkl} = \frac{I_{hkl}/\ I_{0hkl}}{1/\ N \sum_{N=1}^{N} I_{hkl}/\ I_{0hkl}} \quad (6)$$

In this equation, TC_{hkl} stands for the texture coefficient associated with a particular (hkl) plane. The variable I_{0hkl} refers to the intensity observed experimentally for that specific plane, while

I0hkl represents the intensity of the same plane as listed in the standard JCPDS file. N represents the total number of diffraction peaks that are taken into account during the analysis.

The elaboration follows a particular plane direction when the TC_{hkl} value exceeds 1, and it can be considered highly textured if the values exceed 2. The TC_{hkl} values are calculated for the (012), (110), (013) and (104) planes of all films are listed in Table 1. It was observed that the values of the TC_{hkl} texture coefficient for the (012), (110), (013), and (104) directions are greater than 1, confirming a higher number of grains in the preferentially oriented direction. The data presented in Table 1 is analyzed and visualized in Fig. 2. It shows the change in texture coefficient of SnS thin films across different crystallographic planes like (012), (110), (013), and (104), revealing a decrease as the rinsing temperature increases. Additionally, the texture coefficient (TC_{hkl}) is notably higher for the dominant plane (013) compared to the others. It's worth noting that a texture coefficient exceeding 1 indicates a preferential orientation, highlighting the abundance of grains in each direction (h, k, l). Interestingly, the films deposited at 60°C exhibit a higher texture coefficient value compared to those at 70°C and 80°C. This suggests a stronger orientation preference and a higher density of grains in the (013) direction at the lower rinsing temperature.

Table 1. Texture coefficient and preferred orientation grade of the SnS films.

(hkl)	**Texture coefficient**		
	Rinsing temperature		
	60 °C	**70 °C**	**80 °C**
(012)	1,28	1,20	0,73
(110)	1,67	1,38	1,20
(013)	2,28	1,48	1,48
(104)	1,47	0,78	0,59

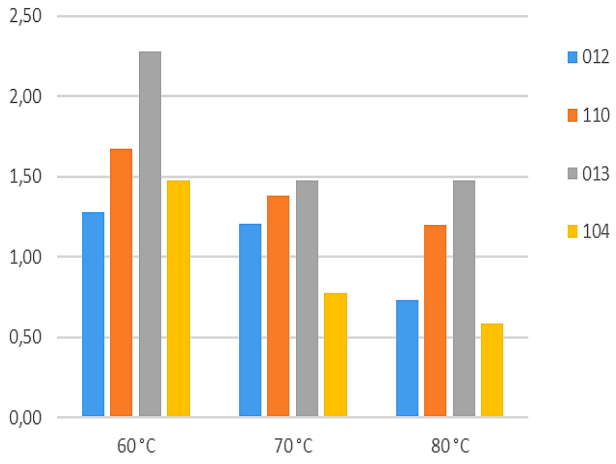

Fig. 2. Histogram of Texture coefficient as a function of SnS various rinsing.

3.2. Morphological studies

In this research, we analyzed the morphological features of SnS samples using Scanning Electron Microscopy (SEM) imaging at a magnification of ×16000. The investigation focused on SnS thin films that were deposited on glass substrates using the SILAR method. Fig.3 illustrates 3 distinct samples of the SnS thin films. In the experimental setup, the glass substrates were uniformly coated with tin sulfide film, exhibiting a nearly uniform size distribution of grains in all samples. Specifically, sample ech1 displayed a rough distribution, characterized by the presence of large flower-like agglomerates of grains on the film's surface, as previously reported [16].

Upon varying the rinsing temperatures during the deposition process, we observed interesting changes in the morphology of the SnS thin films shown in Fig.3. For samples ech2 and ech3, with increased rinsing temperature, there was a noticeable reduction in the compactness of grains compared to sample ech1. The images reveal that the grains became more dispersed and less densely packed, suggesting a correlation between rinsing temperature and grain arrangement.

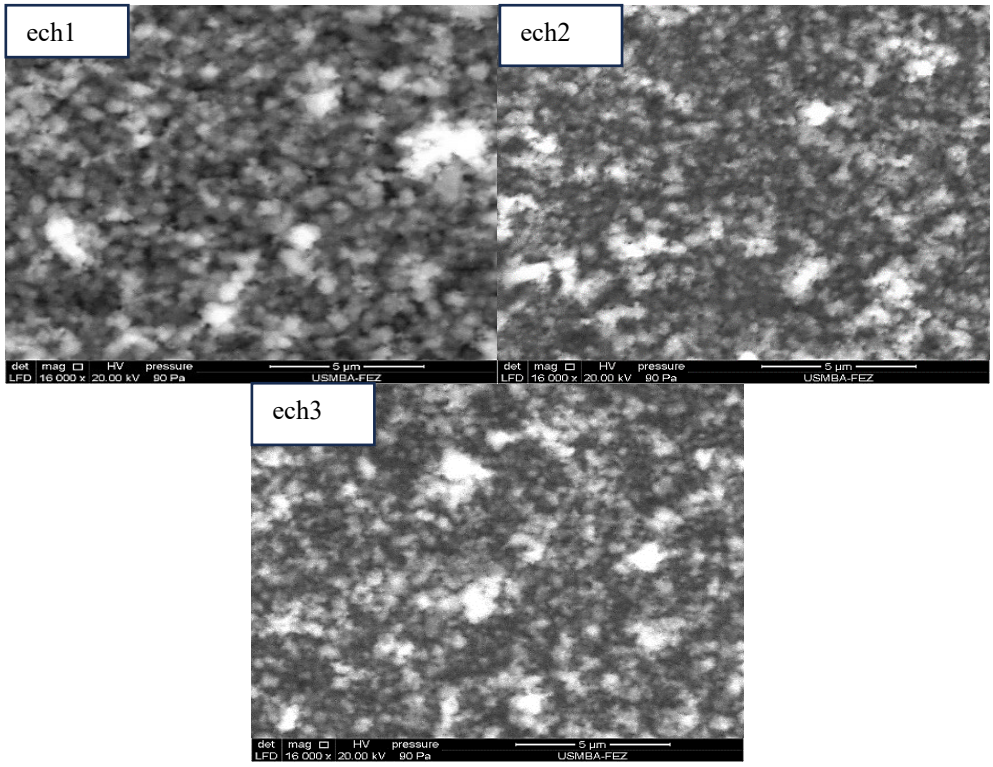

Fig. 3. Scanning electron microscopy images depicting SnS thin films deposited on glass substrates at different rinsing temperatures (ech1-60°C, ech2-70°C, and ech3-80°C).

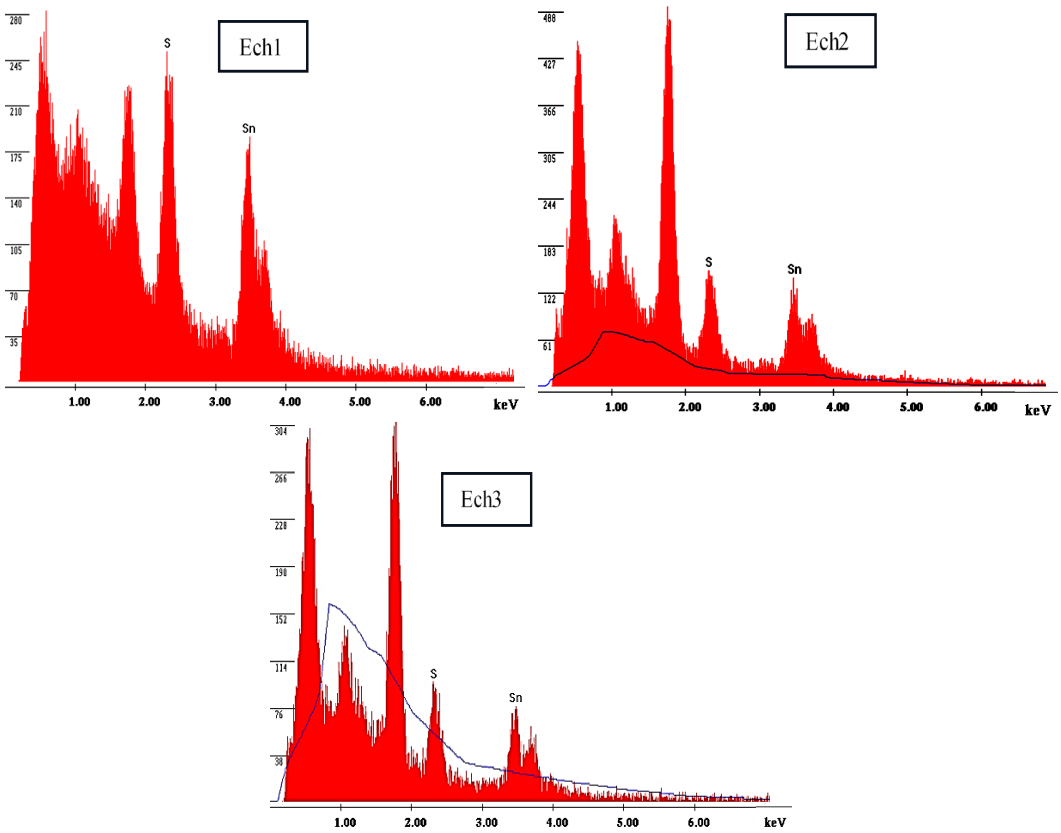

Fig. 4. The EDX spectra reveal the elemental composition of the SnS thin film samples identified as ech1, ech2, and ech3, after deposition.

To determine the elemental composition of the deposited SnS thin films, we conducted a characterization using EDX-SEM. The resulting EDX spectra of the as-deposited thin films are depicted in Fig.4. The elemental analysis reveals the predominant presence of tin (Sn) and sulfur (S) in the samples. Additionally, minor signals corresponding to other elements, notably sodium (Na), chlorine (Cl), silicon (Si), and oxygen (O), were detected, which are attributed to the glass substrate. Upon further examination, we determined the Sn:S ratio for three distinct samples labeled as ech1, ech2, and ech3, with values of 0.88, 0.92, and 0.89, respectively.

This finding indicates that the SnS thin films deposited have an almost perfect stoichiometric composition. The ratios are all close to unity, approximately equal to 1, indicating that the films are slightly enriched in the sulfur component when compared to the tin component.

3.3. Raman studies

Raman scattering tests were performed on newly deposited SnS thin films under room temperature conditions. The analysis unveiled 24 unique vibrational modes that are characteristic of the orthorhombic structure found in SnS [17]:

$$\Gamma = 4A_g + 2B_{1g} + 4B_{2g} + 2B_{3g} + 2A_u + 4B_{1u} + 2B_{2u} + 4B_{3u} \quad (7)$$

The thin film SnS has 21 optical phonons including 12 Raman active modes ($4A_g + 2B_{1g} + 4B_{2g}$ and $2B_{3g}$) [17].

The Raman spectra of SnS thin films recorded at room temperature are presented in Fig.5. These spectra reveal distinct Raman modes, which can be due to the crystalline properties of SnS [18]. Specifically, Distinct Raman peaks are seen at 173,8 cm^{-1}, 199 cm^{-1}, 224 cm^{-1}, and 284 cm^{-1}.

These peaks closely match the Raman modes associated with SnS monocrystalline structures. More specifically, the modes observed at 199 cm^{-1}, and 224 cm^{-1} correspond to the A_g

mode, while those at 173,9 cm^{-1} and 284 cm^{-1} can be linked to the B_{2g} mode. Notably, the agreement between these Raman modes and the XRD (X-ray diffraction) spectra further supports the crystalline nature of the SnS thin films under examination.

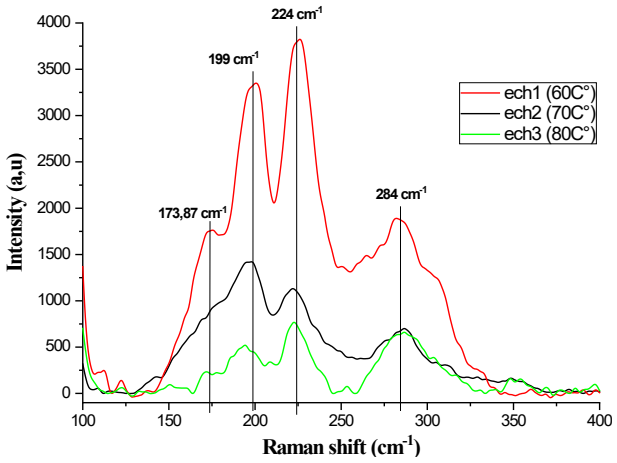

Fig. 5. Raman spectra of SnS films at varying rinsing temperatures.

3.4. Optical studies

Figure 6(a) displays the optical absorbance changes of SnS thin films across the wavelength spectrum of 400 to 1000 nm, deposited under different rinsing temperatures. The prominent absorbance observed in the visible range suggests the potential of SnS thin films as absorber layers.

The theory of optical absorption connects photon energy (hν) and the absorption coefficient (α), as explained in the following manner [12]:

$$\alpha h\nu = A\,(h\nu - E_g)^{n} \tag{8}$$

where the value of n is 2 and 1/2 for direct and indirect transition respectively, A is a constant, hν is the photon energy and E_g the band gap energy. This equation determines band gap (E_g) by extrapolating the linear portion of the $(\alpha h\nu)^2 = f(h\nu)$ graph to intersect the hν axis. We can determine the band gap value for both direct and indirect transitions, as shown in Fig.6 (a) and (b). The linear part of the plot gives a good approximation of the band gap energy. For the direct transitions is found to be 1.58, 1.82 and 1.67 eV and for indirect transitions band gap it's 0.94, 0.78 and 0.63eV for samples ech1, ech2 and ech3 respectively.

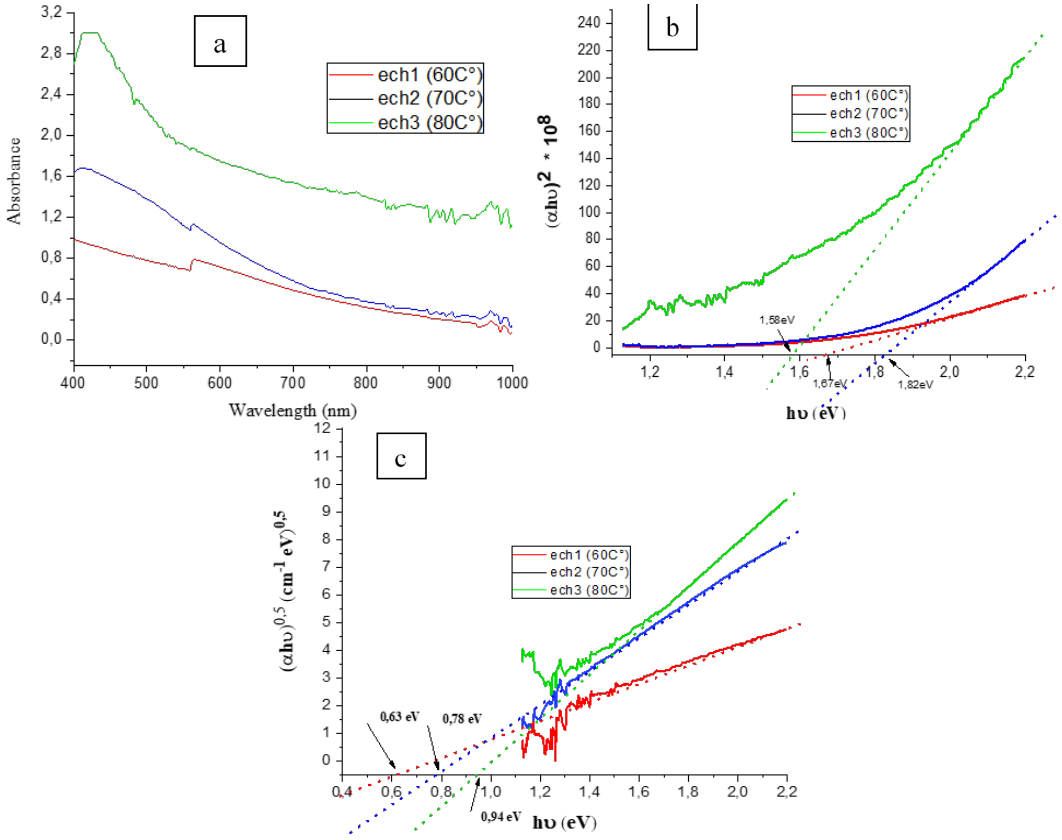

Fig. 6. (a) Optical absorbtion spectra (b) direct bandgap values and (c) The indirect bandgap of SnS thin films fabricated under varying rinsing temperatures.

4. Conclusion

SnS thin films were synthesized on glass substrates via the SILAR method at various rinsing temperatures, highlighting the influence of preparative conditions on film quality. XRD analysis revealed the orthorhombic structure of our SnS thin films, a result further confirmed by Raman spectroscopy, which detected modes corresponding to this structure without secondary phases. SEM images showed a homogeneous grain distribution, and EDX analysis indicated a near-stoichiometric composition with an S:Sn ratio close to 1. The optical band gap, determined via UV-Vis-NIR spectrophotometry, was found to be 1.58, 1.67, and 1.82 eV for direct transitions and 0.63, 0.78, and 0.94 eV for indirect transitions.

References

[1] N. Koteeswara Reddy, ECS J. Solid State Sci. Tech., **2** (6), 259 (2013); http://dx.doi.org/10.1149/2.006306jss
[2] Chao Gao, Honglie Shen, Tianru Wu, Lei Zhang, Feng Jiang, J. of Cryst. Growth **312** (20), 3009 (2010); https://doi.org/10.1016/j.jcrysgro.2010.07.001
[3] W. Albers, C. Haas, H. J. Vink, and J. D. Wasscher, J. App. Phys., **32** (10), 2220 (1961); https://doi.org/10.1063/1.1777047
[4] Meng Cao, Chuangsheng Wu, Kefeng Yao, Jiahe Jing, Jian Huang, Meng Cao, Jijun Zhang, Jianming Lai, Omar Ali, Linjun Wang, Yue Shen, Materials Research Bulletin, **104**, 244 (2018); https://doi.org/10.1016/j.materresbull.2018.03.039
[5] K. Hartman, J.L. Johnson, M.I. Bertoni, D. Recht, M.J. Aziz, M.A. Scarpulla, and T. Buonassisi, Thi. Sol. Fil., **519** (21), 7421 (2011); http://dx.doi.org/10.1016/j.tsf.2010.12.186

[6] F. Jamali-Sheini, M. Cheraghizade, and R. Yousefi, Cur. App Phys., **15** (8), 897 (2015); http://dx.doi.org/10.1016/j.cap.2015.03.026
[7] E. Guneri, C. Ulutas, F. Kirmizigul, G. Altindemir, F. Gode, and C. Gumus, App. Surf. Sci., **257** (4), 1189 (2010); http://dx.doi.org/10.1016/j.apsusc.2010.07.104
[8] R. Mariappan, T. Mahalingam, and V. Ponnuswamy, Optik, **122** (24), 2216 (2011); http://dx.doi.org/10.1016/j.ijleo.2011.01.015
[9] M. Patel, I. Mukhopadhyay, and A. Ray, J. of All. and Comp., **619**, 458 (2015); http://dx.doi.org/10.1016/j.jallcom.2014.08.207
[10] Y. Qachaou, A. Raidou, K. Nouneh, M. Lharch, A. Qachaou, M. Fahoume, L. Laanab, Materials Research Proceedings, **1**, 275 (2016); http://dx.doi.org/10.21741/9781945291197-68
[11] Y. Qachaou, O. Daoudi, A. Raidou, M. Lharch, A. Qachaou, and M. Fahoume, Journal of Physics: Conf. Series **1292** (2019): http://dx.doi.org/10.1088/1742-6596/1292/1/012022
[12] M. Kul, Vacuum, **107**, 213 (2014); http://dx.doi.org/10.1016/j.vacuum.2014.02.005
[13] Hosein Kafashan, Mahdi Azizieh, H. Nasiri Vatan, J. of Alloys and Comps, **686**, 962 (2016); http://doi.org/10.1016/j.jallcom.2016.06.201
[14] Gouranga Maharana, Reddivari Muniramaiah, J. Yuvashree, Diptendu Mandal, Supravat Mondal, M. Kovendhan, Jean Maria Fernandes, Gangalakurti Laxminarayana, D. Paul Joseph, Surfaces and Interfaces, **42**, part A, 103413 (2023); https://doi.org/10.1016/j.surfin.2023.103413
[15] A. Supee, Y. Tanaka, M. Ichimura, Mater. Sci. in Semi Cond. Proc., **38**, 290 (2015); http://doi.org/10.1016/j.mssp.2015.04.028
[16] G.H. Tariq, K. Hutchings, Ghulam Asghar, D.W. Lane, M. Anis-UR-Rehman, Journal of Ovonic Research, **10** (6), 247 (2014); https://api.semanticscholar.org/CorpusID:26854265
[17] Benjamin Hudson Baby, D. Bharathi Mohan, Mater. Chemi. and Phys., **192**, 317 (2017); http://dx.doi.org/10.1016/j.matchemphys.2017.01.078
[18] T. Minemura, K. Miyauchi, K. Noguchi, K. Ohtsuka, H. Nakanishi, and M. Sugiyama, Bull. Korean Chem. Soc., **33** (10), 3383 (2012); http://dx.doi.org/10.5012/bkcs.2012.33.10.3383